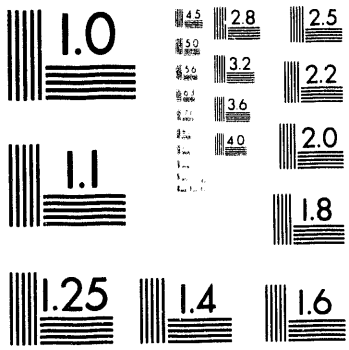
1.0
1.1
1.25
1.4
1.6
1.8
2.0
2.2
2.5
2.8
3.2
3.6
4.0
4.5
5.0

1 of 1

SAND93-0018C

For publication in Proceedings of the ASTM Symposium on Bolted and Bonded Joints in Composite Materials, Nov. 16-17, 1993, Fort Worth, Texas

TESTING COMPOSITE-TO-METAL TUBULAR LAP JOINTS*

T. R. Guess, E. D. Reedy, Jr. and A. M. Slavin
Sandia National Laboratories
Albuquerque, NM 87185

Abstract

Procedures were developed to fabricate, nondestructively evaluate, and mechanically test composite-to-metal tubular joints. The axially loaded tubular lap joint specimen consisted of two metal tubes bonded within each end of a fiberglass composite tube. Joint specimens with both tapered and untapered aluminum adherends and a plain weave E-glass/epoxy composite were tested in tension, compression, and flexure. Other specimens with tapered and untapered steel adherends and a triaxially reinforced E-glass/epoxy composite were tested in tension and compression. Test results include joint strength and failure mode data. A finite element analysis of the axially loaded joints explains the effect of adherend geometry and material properties on measured joint strength. The flexural specimen was also analyzed; calculated surface strains are in good agreement with measured values, and joint failure occurs in the region of calculated peak peel stress.

Key Words: composites, tubular joints, static testing, flexural testing, bonded joints, adhesives, finite element analysis

---

*This work was performed at Sandia National Laboratories and supported by the U.S. Department of Energy under contract DE-AC04-94AL85000.

Introduction

Adhesive bonding is an efficient and convenient method for joining tubular sections. Such joints can be formed from dissimilar materials, and composite-to-metal joints are of particular interest. For example, such joints are found in horizontal axis wind turbine blades where a fiberglass-reinforced resin composite blade terminates as a hollow cylinder that fits onto a metal shaft at the hub. The strength and fatigue resistance of such joints are clearly of importance since failures often occur in the region of joints. A combined experimental/analytical study of bonded tubular joints is being carried out to support Sandia's Wind Energy Technology Department efforts to improve methods to predict the strength and fatigue resistance of joints of the type used in wind turbine blades. Two series of axially loaded, tubular lap joint tests have been performed to date. Thirteen plain weave E-glass fabric/epoxy composite-to-aluminum joints were tested in the First Test Series and the results are documented by Reedy and Guess [1]. In Test Series 2, 16 specimens of triaxially reinforced E-glass/polyester-to-steel joints were tested.

The published literature on adhesively bonded tubular lap joints is reviewed by Reedy and Guess [1]. Notable recent work on this topic include that of Whitcomb and Koo [2] and Shi and Cheng [3]. This paper describes the experimental program to fabricate, inspect, and test composite-to-metal tubular joints. Test results from Test Series 1 are reviewed and the Test Series 2 data are presented. Finite element analyses are used to interpret trends observed in the experimental data. This paper also discusses experimental and analytical results for Series 1-type tubular lap joints subjected to flexure.

Experimental Procedures

Joint Specimen

Axial Specimen--A schematic of the tubular joint specimen used for all axial loading conditions is shown in Fig. 1. Each specimen actually contains two adhesively bonded lap joints; one at each end. The outer adherend is an E-glass composite tube and the two inner adherends are metal tubes. The specimen is axisymmetric with a plane of symmetry at mid length. Both adherend joints in a specimen are equally loaded during a test and failure occurs in the weaker joint. Therefore, reported strengths are representative lower bounds.

The composite tube has a nominal outer diameter of 76.2 mm, a wall thickness of 6.35 mm and a length of 305 mm. The metal adherends have an outer diameter of approximately 63.5 mm, a wall thickness of 12.5 mm and a length of 152.3 mm. The nominal length and thickness of the adhesive bond are 76 mm and 0.25 mm, respectively. The bond end located 76 mm from the end of the composite tube is called the inner bond end (see Fig. 1), and is the location where bond failure initiates in the axial tests. In some specimens the metal adherend is tapered at the inner

bond end and in the other specimens there is no taper. The outer ends of the metal adherends are internally threaded to facilitate attachment to the load-train.

Flexural Specimen--Flexural specimens are identical to the axial specimens (see Fig. 1), with the exceptions that there is only one metal adherend and the composite tube is 762 mm long.

Materials

Table 1 lists the materials and their elastic properties. For the thirteen Series 1 axial specimens and two flexural specimens, the outer adherend is a plain weave (style 7628) E-glass fabric/epoxy composite tube, referred to commercially as G10. This material has 42% of the glass reinforcement oriented in the axial direction and 58% in the hoop direction. Axial elastic properties were measured for the composite with strain gages and an extensometer in the uniformly stressed region of the lap joint specimen. Young's modulus is 22.5 GPa and Poisson's ratio ($\nu_{axial\text{-}hoop}$) is 0.17. Series 1 specimens had 6061-T6 aluminum inner adherends (Young's modulus of 69 GPa and a Poisson's ratio of 0.33). The bonding material is Hysol EA-9394, a high strength, room-temperature curing paste adhesive. As processed in these specimens, this adhesive is a nonhomogeneous, filled material. Adhesive properties were measured using strain gaged, cast adhesive dog-bone specimens tested in tension, and cylindrical specimens (height/diameter = 2) tested in axial compression. EA-9394 has a Young's modulus of 4 GPa, a Poisson's ratio of 0.35, and its yield behavior can be reasonably modeled as elastic-perfectly plastic with a 63.5 MPa yield strength. Both the inner and outer surfaces of the Series 1 composite tubes are smooth. The smooth outer surface permits the use of ultrasonic C-scans to inspect joint bondlines for debonds and voids.

There were sixteen Series 2 specimens. The outer adherend is a triaxially reinforced E-glass/polyester tube. The triaxially reinforced composite tubes contains unidirectional layers stitched together with 70% of the glass reinforcement oriented in the axial direction and 15% in each of the ±45° directions. The measured axial Young's modulus is 21.0 GPa, and Poisson's ratio ($\nu_{axial\text{-}hoop}$) is 0.40. The inner metal adherends are 1018 steel with a Young's modulus of 200 GPa and a Poisson's ratio of 0.30. This composite is more representative of the materials and fabrication processes used in wind turbine blades than the Series 1 composite. The inner surface of this tube is smooth because of a polyester rich surface; however, the outer surface is very rough and lacks a resin rich surface. The bonding material is the same Hysol EA-9394 paste adhesive used in the Series 1 specimens.

Assembly and Inspection

The joint specimens were fabricated using a method that carefully controls the bondline thickness and also minimizes bondline voids within the bond. Six to eight spacers of 3 mm

diameter are used to establish the bondline thickness and also to center the metal adherends within the outer composite tube. Elastomeric dams are placed at the ends of the composite tube to fix the outer end of the bondlines. The adhesive is injected through three fill holes on each end of the outer composite adherend until the adhesive just begins to flow out of the inner end of the bondline in a circumferentially uniform manner. The fill holes are 120° apart and are positioned 12 mm from the tube ends. Ultrasonic, C-scan methods were used to inspect for complete bondline filling in all Series 1 and flexural specimen composite-to-metal joints prior to testing. The bondline of Series 2 specimens could not be inspected by C-scan methods because of excessive outer surface roughness. These joints were visually inspected for adhesive filling by taking advantage of the translucent nature of the triaxially reinforced E-glass/polyester material. However, visual inspection is not sensitive enough to discern cracks in the adhesive bondline.

Test Procedures

The joint specimens are loaded in a 450 kN servo-hydraulic test frame for the axial tests. Universal joints are used on both ends of the load train, and the metal adherends are attached to the universal joints by threaded rods. Many of the specimens are strain gaged, and all are instrumented with a 50 mm extensometer at the specimen's midplane (in the uniformly stressed region of the composite tube) to measure the composite's axial stress-strain relation. Specimens are tested under monotonically increasing or decreasing load increments until one of the two joints fails. Load and strains are recorded at each load increment.

Fig. 2 shows a schematic of the experimental configuration for the flexural tests and specimen dimensions. The aluminum adherend is rigidly clamped, and a bending load is applied at the end of the composite tube through a Kevlar strap. Strain gages were located both over and beyond the lap joint region. The specimen was subjected to loading-unloading cycles with a monotonically increasing maximum load. Load, strain, and tube-end deflection measurements were recorded, and a portable ultrasonic unit was used to inspect the bondline at the end of each cycle.

Test Results

Series 1 Axial Specimens

The data for Series 1 specimens were previously reported [1], and are summarized here for completeness. Table 2 lists the measured tensile joint strength for six specimens with untapered aluminum adherends and two specimens with tapered adherends. Table 3 lists compression joint strength results for three specimens with untapered aluminum adherends and two specimens with tapered adherends. The applied load is characterized in terms of τ, the average shear stress in the bond (equals absolute value of the applied load in Newtons divided by the shear area of the bond),

and in the following, joint strength of axially loaded specimens is always specified in this way. For specimens with untapered aluminum adherends, measured joint tensile strength varies from 14 to 21 MPa, with an average of 16.4 MPa, while the average compressive strength is only 10.4 MPa (less than 65% the tensile strength). For specimens with tapered aluminum adherends, the average tensile and compressive strengths are 11.6 MPa and 12.0 MPa, respectively. These results, displayed graphically in Fig. 3, suggest that the joint tensile strength is greater than the joint compressive strength for untapered aluminum adherends, while the joint tensile strength is roughly the same as joint compressive strength for tapered aluminum adherends. This latter influence is not conclusive, however, since the test data are limited. Taper appears to decrease joint tensile strength, but increase joint compressive strength. In all tests, the specimen fails abruptly with no preliminary load drop. Recall that each test specimen contains two adhesively bonded joints. At maximum load the weaker of the two joints fails completely, allowing the unbonded aluminum adherend to slide relative to the plain weave E-glass fabric/epoxy composite tube.

Features of the subcritical adhesive failure process of the Series 1 specimens were identified by ultrasonically C-scanning and sectioning the unfailed specimen end. Adhesive failure initiates at the inner bond end (i.e., where the metal adherend terminates). A section taken from a specimen tested in tension shows cohesive failure with a single crack within the failed adhesive, roughly parallel and close to, but not on, the interface.

Series 2 Axial Specimens

The data for Series 2 specimens have not been previously reported. Table 4 lists the measured tensile joint strength for four specimens with untapered steel adherends and four specimens with tapered adherends and Table 5 contains compressive joint strengths of four specimens with untapered steel adherends and four specimens with tapered adherends. For specimens with untapered steel adherends, average measured joint tensile strength is 12.8 MPa and the average compressive strength is 5.6 MPa. Likewise, for specimens with tapered steel adherends, the average tensile and compressive strengths are 12.8 MPa and 7.6 MPa, respectively. These Series 2 data, shown in Fig. 4, suggest that the average tensile strength of tubular joints with untapered steel adherends is equivalent to the tensile strength of joints with tapered steel adherends. There also appears to be little difference in the compressive strength of joints with untapered and tapered steel adherends. Note, however, the compressive strength is only about 50% the tensile strength, for both tapered and untapered steel adherends.

As indicated previously, the surface texture of the triax weave composite in the Series 2 specimen is too irregular to inspect for subcritical adhesive failure using ultrasonic C-scan methods. Based on the bondline stress state (to be discussed later in the analysis section), adhesive failure most likely initiates at the inner bond end of the joint. Visual examination of the

bondline surface of the steel adherend pulled from the failed joint reveals that the fracture appears to grow on or near the composite-to-adhesive interface. In tensile specimens, the steel adherend was covered with EA-9394 adhesive (which suggests failure at the composite-to-adhesive interface) and polyester and E-glass fiber debris (which suggests failure in the composite near the composite-to-adhesive interface). It is important to understand that only small amounts of composite pull out during joint failure and there is no large scale fracture of the composite.

Flexural Specimens

The first flexural test specimen failed at a load of 3580 N and the second at 6230 N. Specimen 1 was subjected to five loading-unloading cycles with the maximum load increased by 890N each cycle, while specimen 2 was subjected to fourteen loading-unloading cycles with the maximum load increased by 445N each cycle. Failure was accompanied by a loud audible pop and a significant drop in applied load. A hand held portable ultrasonic device was used to inspect the bondline. Based on ultrasonic inspection of the bondline on the composite's compression side, there was no subcritical crack growth in the first specimen prior to joint failure. In the second specimen, a crack of about 6 mm length was detected in the bondline during the load increment just prior to joint failure. The debond was near the inner adherend end of the joint on the compression side of the composite tube.

Fig. 5 is a schematic of joint debond regions mapped by ultrasonic C-scans following the flexural tests. The first specimen has bondline failure in only one region; whereas, the second specimen has two failure locations, one on the compression side at the inner bond end, and one on the tensile side at the outer bond end. Following the tests, the joints were sectioned for microscopic examination. Sectioned samples reveal bondline failures in the regions indicated by the C-scans. Specimen 1 failure initiated in the composite near the inner bond end at a distance of roughly 0.10 mm below the composite surface. After it runs a little more than 1 mm, the crack moves from within the composite to the composite/adhesive interface. Apparently, there is a weak region in the composite causing the joint to fail at the low load of 3580 N. Inspection of sectioned samples of Specimen 2 suggests that cohesive failure occurs in the EA-9394 paste adhesive very near the adhesive/aluminum adherend interface; there is no failure in the composite. The different failure initiation sites are most likely the reason for the wide spread in the failure loads between the first specimen (3580 N) and the second specimen (6230 N).

The second flexural specimen has two debond regions. Surface strain measurements in the joint region suggest that the debond failure on the compression side of the tube occurred before the debond failure on the tension side. The load-strain response of a strain gage located nearest the debond region on the tension side was continuous at all load increments up to failure. On the other hand, the response of a strain gage located near the debond region on the compression side

had a discontinuity at load increments just prior to joint failure. This discontinuity may be indicative of subcritical crack growth in the bondline, and that first failure began in this region.

Analysis

Axially Loaded Joint Specimens

Calculations have been carried out to investigate how tapering the metal adherend effects bond stresses in axially loaded joints, and results for a plain weave E-glass fabric-to-aluminum joint (Series 1 specimen) are compared with results for a triaxially reinforced E-glass fabric/polyester-to-steel joint (Series 2 specimen). The analysis models the adhesive as an unflawed (uncracked), elastic-plastic material. This is one of the two different approaches previously used to analyze Series 1 specimens when results for those joint specimens were initially reported (a fracture mechanics approach was also used) [1].

Fig. 1 defines the geometry of the axially loaded, tubular lap joint specimen. The specimen geometry and the applied loading are axisymmetric, and the specimen is also symmetric about its midplane. Accordingly, axisymmetric finite element analyses were performed (using Version 4-9 of the ABAQUS finite element code [4]) with midplane symmetry conditions applied. The joint was loaded by axially displacing the end of the metal adherend. Table 1 lists material properties used in the analysis. The metal inner adherend and the E-glass composite outer adherend were both modeled as linear elastic materials. The E-glass composite outer adherend was modeled as orthotropic elastic. Note that only the axial composite properties were measured. Other E-glass composite properties were estimated using known unidirectional properties and fabric construction. The finite element analysis used a standard elastic-perfectly plastic model for the adhesive with a von Mises yield surface and associated plastic flow rule. Since the adhesive bond was cured at room temperature to minimize residual fabrication stresses, these stresses were not included in the analysis.

Fig. 6 shows an example of the finite element mesh used to analyze an axially loaded joint specimen. The bond has four elements through its thickness, and the mesh is refined at the bond ends where the highest stress gradients are expected (the 75 mm bond length used in this mesh is an approximation of the 76.2 mm length indicated in Fig. 1). This mesh contains 4150, 4-node, axisymmetric elements (CAX4 elements).

Fig. 7 plots calculated effective (von Mises) stress, σ_e, in the adhesive along the composite/adhesive interface for τ = 10.6 MPa (this load level is representative of typical failure loads, see Tables 2-5). Results are presented for Series 1 and 2 specimens with metal adherends that were either tapered or untapered (taper defined in Fig. 1). Note, all plotted stress distributions are defined along a line parallel to, but offset from, the composite/adhesive interface. The offset distance is equal to one eighth the bond thickness (i.e., the stress calculated in elements

adjacent to the interface). Also note that distance along this line is measured relative to the outer bond end (see Fig. 1). Differential adherend straining elevates the shear stress at the ends of the bond. Furthermore, differential straining is magnified when there is an imbalance in adherend stiffness. The calculated effective stress distributions in Fig. 7 reflect the effect of differential straining with the highest effective stress at the inner bond end where the less stiff E-glass composite adherend extends. The calculated effective stress distribution manifests bond yielding at the inner bond end (yielding occurs when σ_e = 63.5 MPa), and one expects cracking to initiate in the region of highest plastic strains. Recall that in all tests, bond failure initiated at the inner bond end. Note, however, calculated effective stress distributions are the same for both axial tensile and compressive loadings. Consequently, the experimentally observed differences in joint tensile and compressive strength cannot be solely explained in terms of effective stress distributions.

The bond is also subjected to a radial (bond normal or peel) stress (Fig. 8). Tubular end-moments generated by bondline shear stress and Poisson's ratio effects combine to create deformations that are resisted by radial adhesive stress. Peak values of the calculated radial stress must be interpreted carefully. In the region where the bond terminates, over a distance of the order of the bond thickness, the shear stress quickly decays to satisfy the stress-free condition at the end of the bond. A very complex stress state exists in this region, and within the context of continuum mechanics, stress and strain singularities can exist at points where an interface intersects the free surface. Consequently, stresses calculated using a relatively coarse mesh and standard finite element techniques cannot be considered reliable within roughly one adhesive thickness (0.25 mm) of the bond end. Nevertheless, the results presented here indicate that the radial bond stress at the inner bond end (where the bond is plastically deformed, see Fig. 7) is quite high over a distance of the order of tens of bond thickness. Note that the sign of the radial stress depends on the sign of the applied joint load. For example, for a Series 1 specimen with an untapered adherend, the radial stress is compressive for an applied tensile joint load, and is tensile for an applied compressive joint load. The calculated peel stress at the inner bond end of both tapered and untapered steel adherend Series 2 specimens exhibits similar behavior. This may explain why the measured joint compressive strength for these joint specimens is less than their tensile strength (see Figs. 3 and 4). Presumably, crack initiation in the plastically deforming adhesive occurs more readily in the presence of a tensile radial (bond normal) stress. In contrast to the other joint specimens analyzed, the calculated peel stress at the inner bond end of a Series 1 specimen with a tapered aluminum adherend is tensile for a tensile joint loading. The experimental results also suggest that adherend taper altered the strength differential effect in Series 1 specimens (see Fig. 3). However, the measured strengths of the four Series 1 specimens with tapered aluminum adherends exhibited substantial scatter (Table 2-3), preventing a conclusive determination.

Flexurally Loaded Joint Specimens

Calculations have been carried out to investigate the nature of the strain distribution found in the tested flexure joint specimens. Although the flexure joint specimen is geometrically axisymmetric, the loading has only one plane of symmetry. Accordingly, a three-dimensional finite element model was developed. As seen in Fig. 2, the major dimensions of the flexure joint specimen are on the order of hundreds of millimeters, while the bond thickness is only a quarter of a millimeter. This large difference in characteristic dimensions can lead to prohibitively large finite element models if only solid elements (i.e., continuum elements) are used. Nevertheless, solid elements are desirable to fully capture the behavior of the bond layer. For this reason, an approach that ties shell elements of the composite and aluminum tubes to solid elements of the bond layer was developed. The shell element nodes defining the mid-planes of the composite and aluminum tubes are tied to the nodes defining the surface of the bond layer using MPCs (Multi-Point Constraints). The accuracy of this approach was investigated by analyzing a cantilever beam with a concentrated end load. The results were in good agreement with those obtained using analytical solutions. In addition, the flexure model was loaded axially, and the bond stresses were compared to those obtained using the axisymmetric analysis described above. Again, good agreement was obtained.

A fully elastic analysis of the flexure joint model was performed. This model uses the Series 1 (plain weave E-glass fabric bonded to aluminum) properties listed in Table 1. The composite and aluminum tubes were modeled using the ABAQUS S4R shell element, a reduced integration four-node "thick shell" element, allowing transverse shear deformation [5]. The bond was modeled using the C3D8 solid element, an eight-node, linear element. The ABAQUS "BEAM" MPC was used to simulate a rigid beam placed between the constrained nodes. Fig. 9 shows the finite element mesh in the bond region. The complete model uses 8080 shell elements to model the composite tube (3920 in the bond region, 4160 beyond the bond region), 7840 solid elements to model the bond layer, and 3920 shell elements to model the aluminum tube.

Recall that axially oriented strain gages were used to measure the strains at the outer surface of the E-glass composite during the flexure tests. Fig. 10 compares the normalized calculated axial strain distribution on the top and bottom of the composite tube with the normalized data obtained at the lowest test load. Data shown is from both the compressive and tensile loaded portions of the E-glass. Note that the "notch" in the calculated strain distribution is associated with localized bending where the E-glass tube extends beyond the aluminum adherend. The calculated results and data are in good agreement, suggesting that the model should provide a reasonable estimate of bond stress. Fig. 11 plots the axial distribution of the normalized effective (von Mises) stress in the bond elements adjacent to the composite at the top of the tube. As before, distance is

measured relative to the outer bond end. The stress analysis predicts formation of a measurable yield zone at roughly 40 percent of the highest test load (second test). Fig. 12 shows the distribution of the normalized peel stress along the upper, compressively loaded portion of the tube. High tensile peel stress occurs at the inner bond end. A similar stress distribution with opposite sign is obtained along the lower, tensile loaded portion of the tube, with high tensile peel stress at the outer bond end. Note that the calculated regions of high tensile peel stress correspond to the observed failed regions shown in Fig. 5.

Conclusions

- Adhesive debonding at the inner bond end is the primary joint failure mode for both axial tension and axial compression monotonic loadings.
- The axial strength of composite-to-metal joints for a compression loading can differ significantly from that for tensile loading. Relative joint strength correlates with the peel (pinch) stress found at the inner bond end.
- Joints subjected to flexural loading also fail in the region of elevated peel stress.
- Finite element analysis is an excellent tool for quantifying the effect of material and joint design choices on the peel stresses that control the strength of composite-to-metal joints.

References

[1] Reedy, E.D., Jr., and Guess, T.R., "Composite-to-Metal Tubular Lap Joints: Strength and Fatigue Resistance", to be published International Journal of Fracture.

[2] Whitcomb, J.D. and Woo, K., "Analysis of Debond Growth in Tubular Joints Subjected to Tension and Flexural Loads", Composites and Structures, Vol. 46, 1993, pp. 323-329.

[3] Shi, Y. P. and Cheng, S., "Analysis of Adhesive-Bonded Cylindrical Lap Joints Subjected to Axial Load", Journal of Engineering Mechanics, Vol. 119, No. 3, March 1993, pp. 584-602.

[4] ABAQUS Version 4-9, Hibbitt, Karlsson, and Sorensen, Providence, Rhode Island (1989).

[5] ABAQUS Version 5-2, Hibbitt, Karlsson, and Sorensen, Pawtucket, Rhode Island (1992).

List of Tables

Fig. Captions

Table 1--Materials and properties.

Material	Modulus (GPa)			Poisson's Ratio			Shear Modulus (GPa)		
	Axial	Hoop	Radial	Radial-Axial	Radial-Hoop	Axial-Hoop	Radial-Axial	Radial-Hoop	Axial-Hoop
Series 1 Joint									
Plain Weave E-Glass Fabric/Epoxy Composite	22.5	28.0	10.0	0.10	0.10	0.17	5.0	5.0	5.0
6061-T6 Aluminum	69.0	69.0	69.0	0.33	0.33	0.33	26.0	26.0	26.0
Hysol EA-9394 Adhesive	4.0	4.0	4.0	0.35	0.35	0.35	1.5	1.5	1.5
Series 2 Joint									
Triax Reinforced E-Glass/Polyester Composite	21.0	7.5	6.0	0.10	0.30	0.40	4.0	4.0	4.0
1018 Steel	200.0	200.0	200.0	0.30	0.30	0.30	77.0	77.0	77.0
Hysol EA-9394 Adhesive	4.0	4.0	4.0	0.35	0.35	0.35	1.5	1.5	1.5

Note 1. Series 1 composite has fiber orientation as follows- 42% in axial direction and 58% in hoop direction.

Note 2. Series 2 composite has fiber orientation as follows- 70% in axial direction, 15% at +45 degrees and 15% at - 45 degrees.

Table 2--Tensile joint strength of Series 1 specimens with tapered and untapered aluminum adherends.

Untapered Aluminum Adherends			Tapered Aluminum Adherends		
Specimen ID	Failure Load (kN)	Shear Strength (MPa)	Specimen ID	Failure Load (kN)	Shear Strength (MPa)
T-1	209	13.8	GT-1	123	8.1
T-2	309	20.3	GT-2	231	15.2
T-3	231	15.2			
T-4	211	13.9			
T-5	312	20.5			
GNT-1	219	14.4			
Average	249	16.4	Average	177	11.6
Standard Deviation	49	3.2			

Table 3--Compression joint strength of Series 1 specimens with tapered and untapered aluminum adherends.

Untapered Aluminum Adherends			Tapered Aluminum Adherends		
Specimen ID	Failure Load (kN)	Shear Strength (MPa)	Specimen ID	Failure Load (kN)	Shear Strength (MPa)
C-1	-156	10.2	GT-3	-159	10.4
C-2	-154	10.1	GT-4	-205	13.5
GNT-2	-164	10.8			
Average	-158	10.4	Average	-182	12.0

Table 4--Tensile joint strength of Series 2 specimens with tapered and untapered steel adherends.

Untapered Steel Adherends			Tapered Steel Adherends		
Specimen ID	Failure Load (kN)	Shear Strength (MPa)	Specimen ID	Failure Load (kN)	Shear Strength (MPa)
TT3	173	11.7	TT1	231	15.6
TNT1	211	14.2	TT5	145	9.7
TNT2	189	12.7	TT8	173	11.6
TNT6	186	12.5	TT9	214	14.4
Average	190	12.8	Average	191	12.8
Standard Deviation	16	1.1	Standard Deviation	39	2.7

Table 5--Compression joint strength of Series 2 specimens with tapered and untapered steel adherends.

Untapered Steel Adherends			Tapered Steel Adherends		
Specimen ID	Failure Load (kN)	Shear Strength (MPa)	Specimen ID	Failure Load (kN)	Shear Strength (MPa)
TNT3	-89	6.0	TT2	-98	6.6
TNT4	-82	5.5	TT4	-127	8.5
TNT5	-78	5.2	TT6	-116	7.8
TNT7	-82	5.5	TT7	-111	7.5
Average	-83	5.6	Average	-113	7.6
Standard Deviation	5	0.3	Standard Deviation	12	0.8

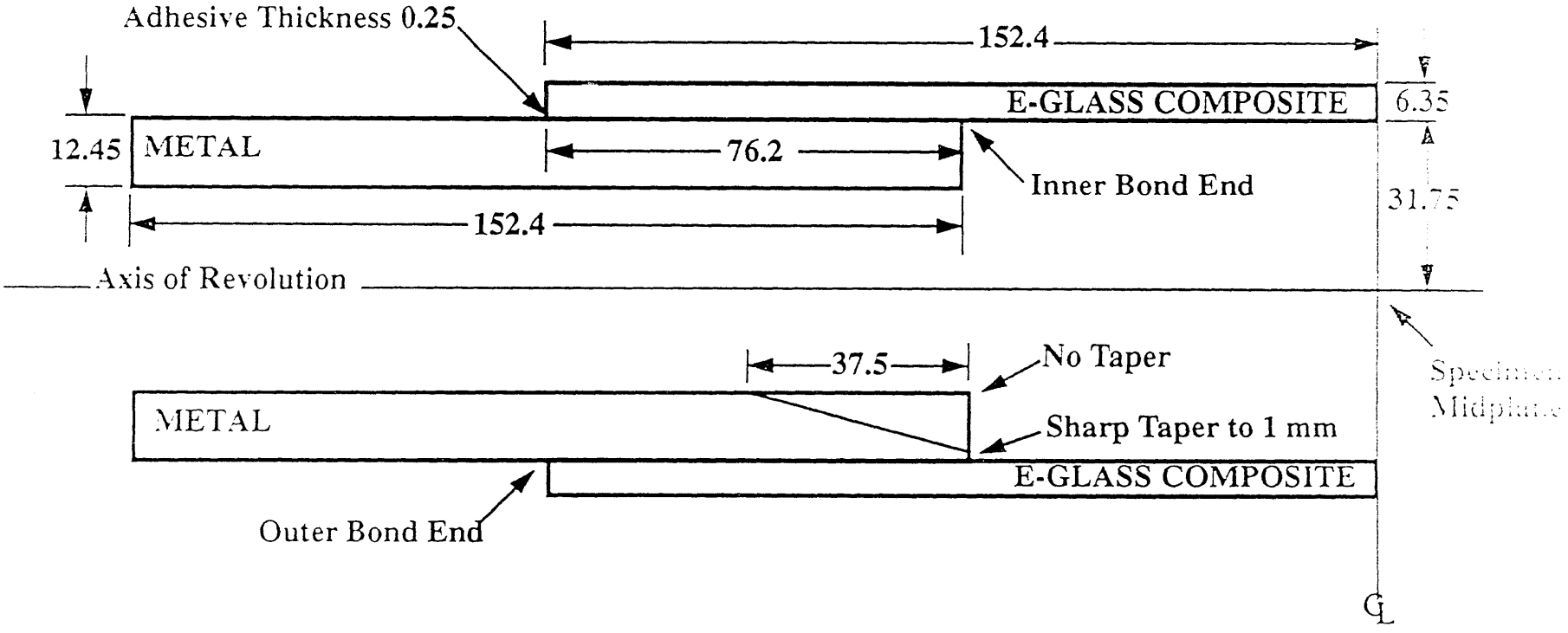

Fig. 1. E-glass composite-to-metal tubular lap joint specimen used in axial loading tests (dimensions in mm).

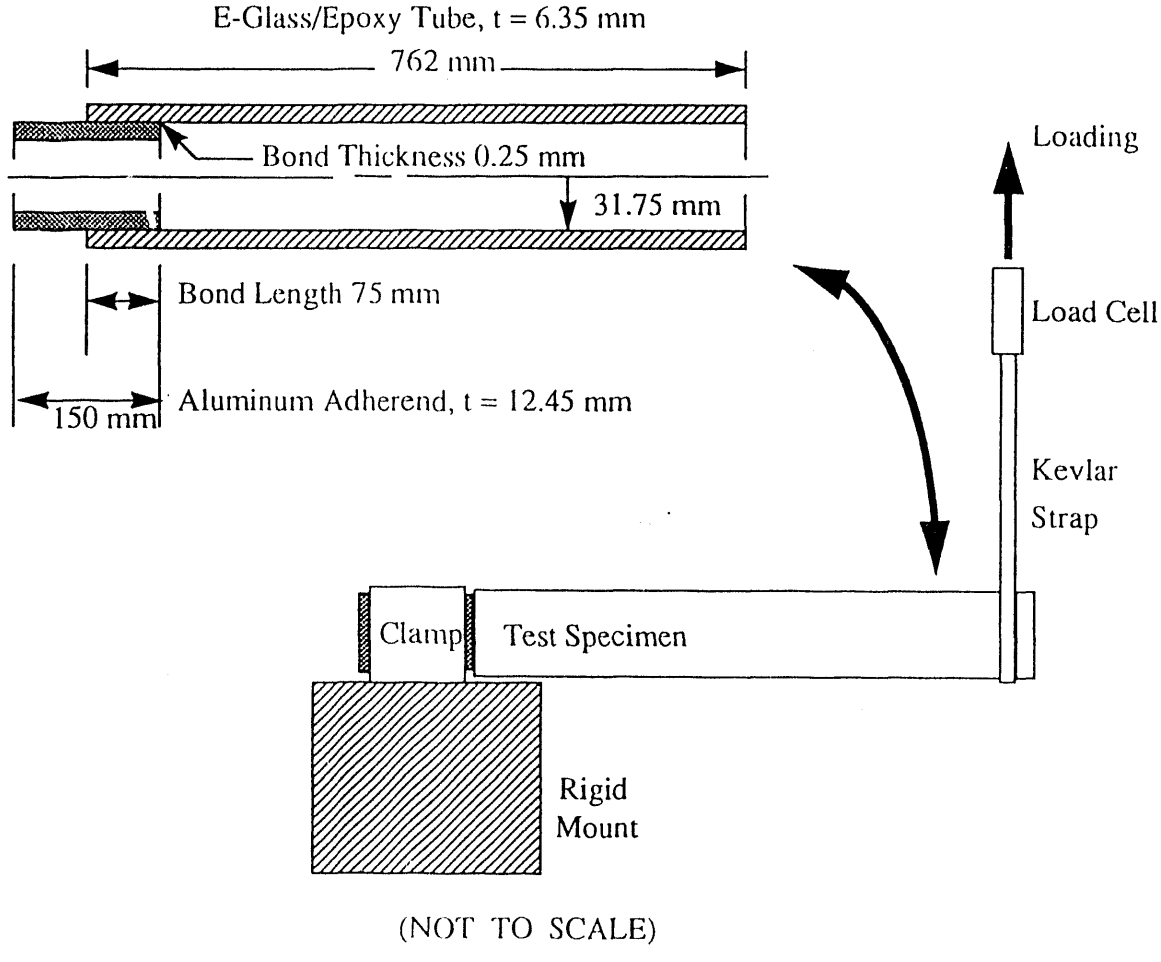

Fig. 2. Flexural test setup and specimen dimensions.

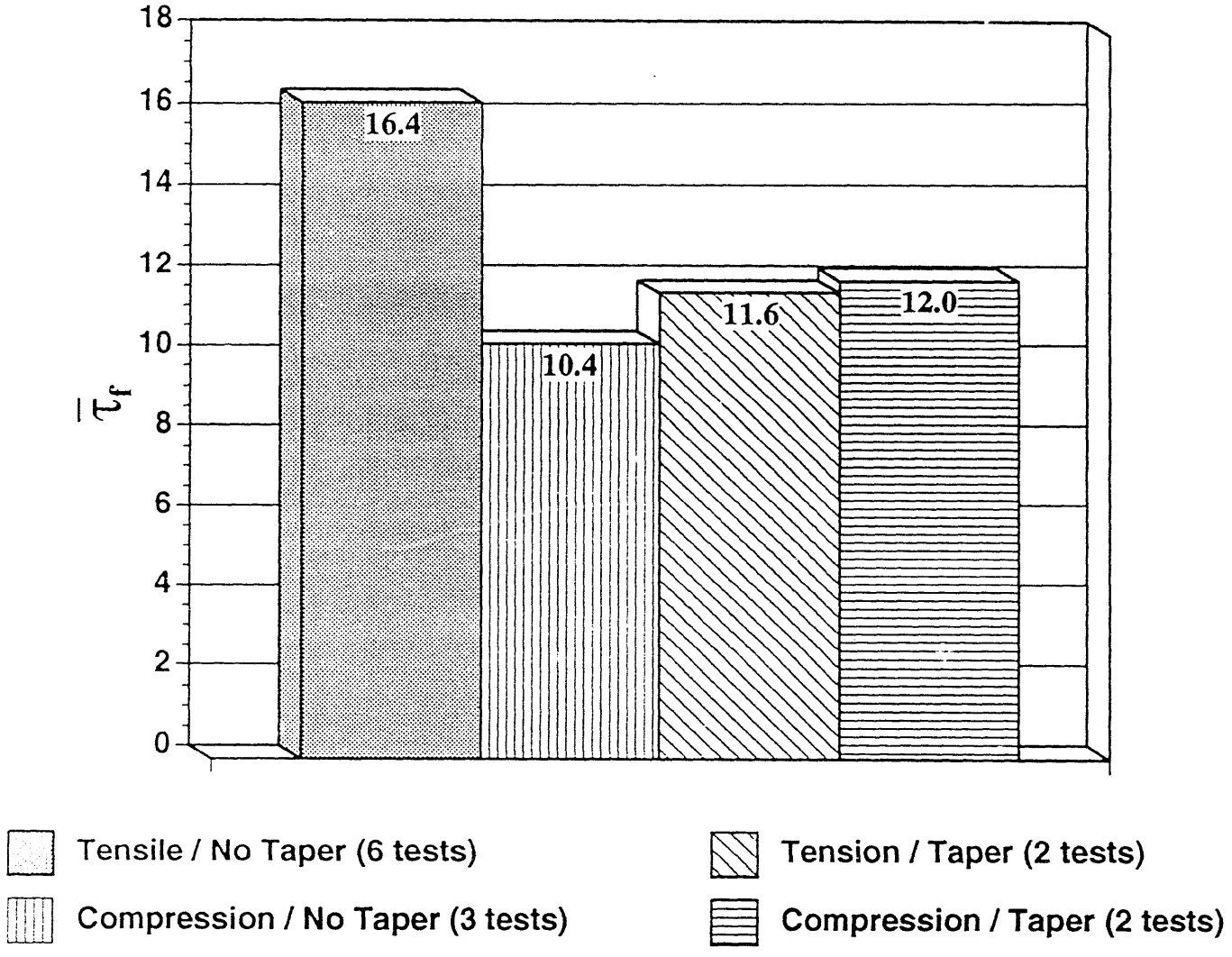

Fig. 3. Joint strength of Series 1 specimens versus aluminum adherend taper. The composite is a plain weave E-glass fabric/epoxy and the axial loading was monotonic. (Data from Reedy and Guess [1]).

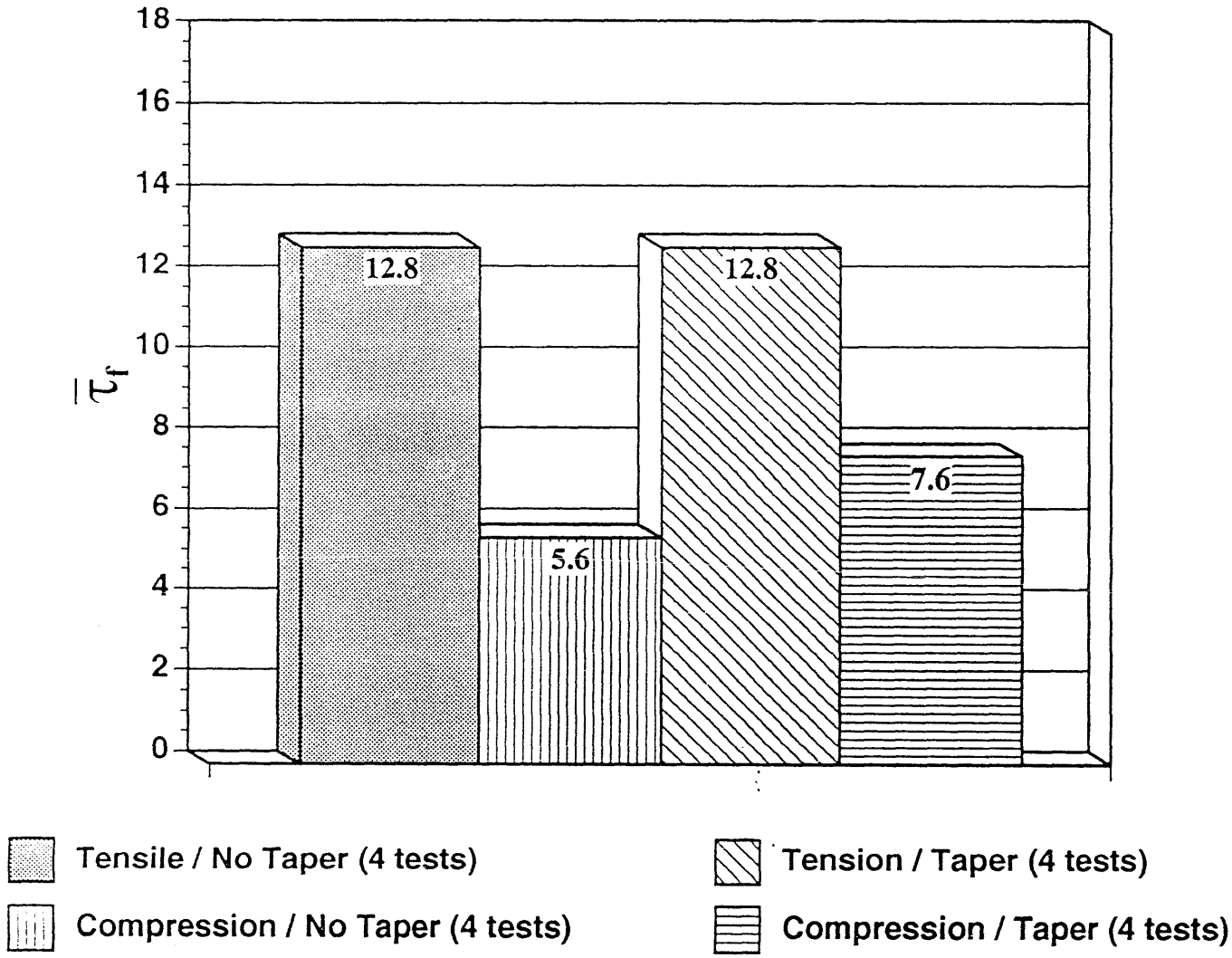

Fig. 4. Joint strength of Series 2 specimens versus steel adherend taper. The composite is triaxially reinforced E-glass/polyester and the axial loading was monotonic.

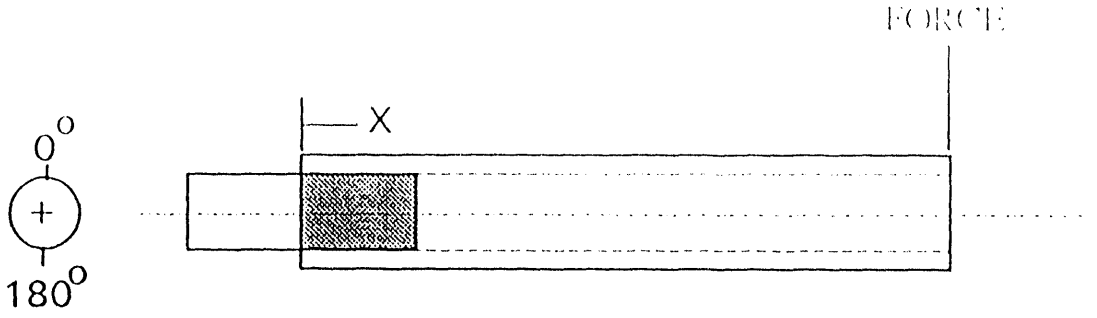

(a) Flexural joint specimen

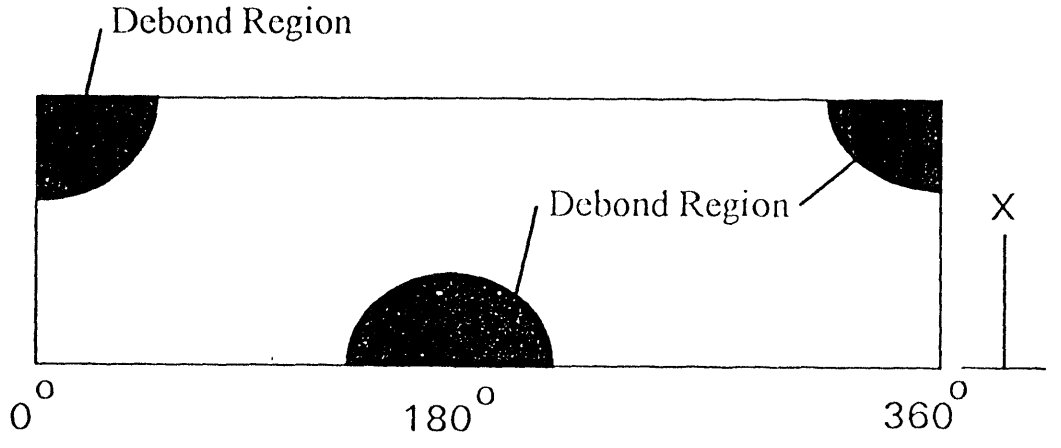

(b) C-scan of joint

Fig. 5. Schmetic of failure locations in second flexural specimen- (plain weave E-glass/epoxy outer adherend and untapered aluminum inner adherend).

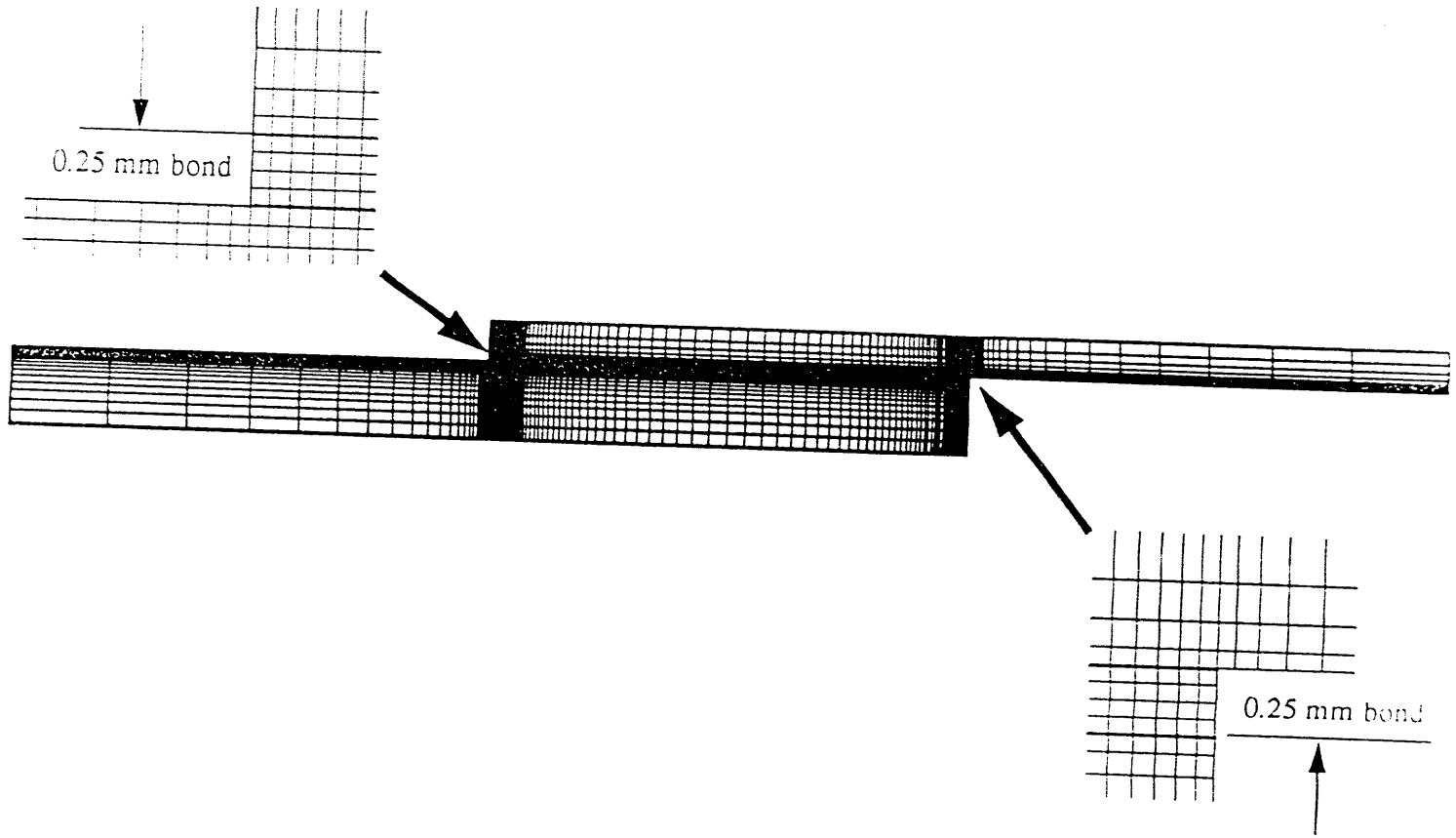

Fig. 6. Example of finite element mesh used to analyze the axially loaded, tubular lap joint specimen.

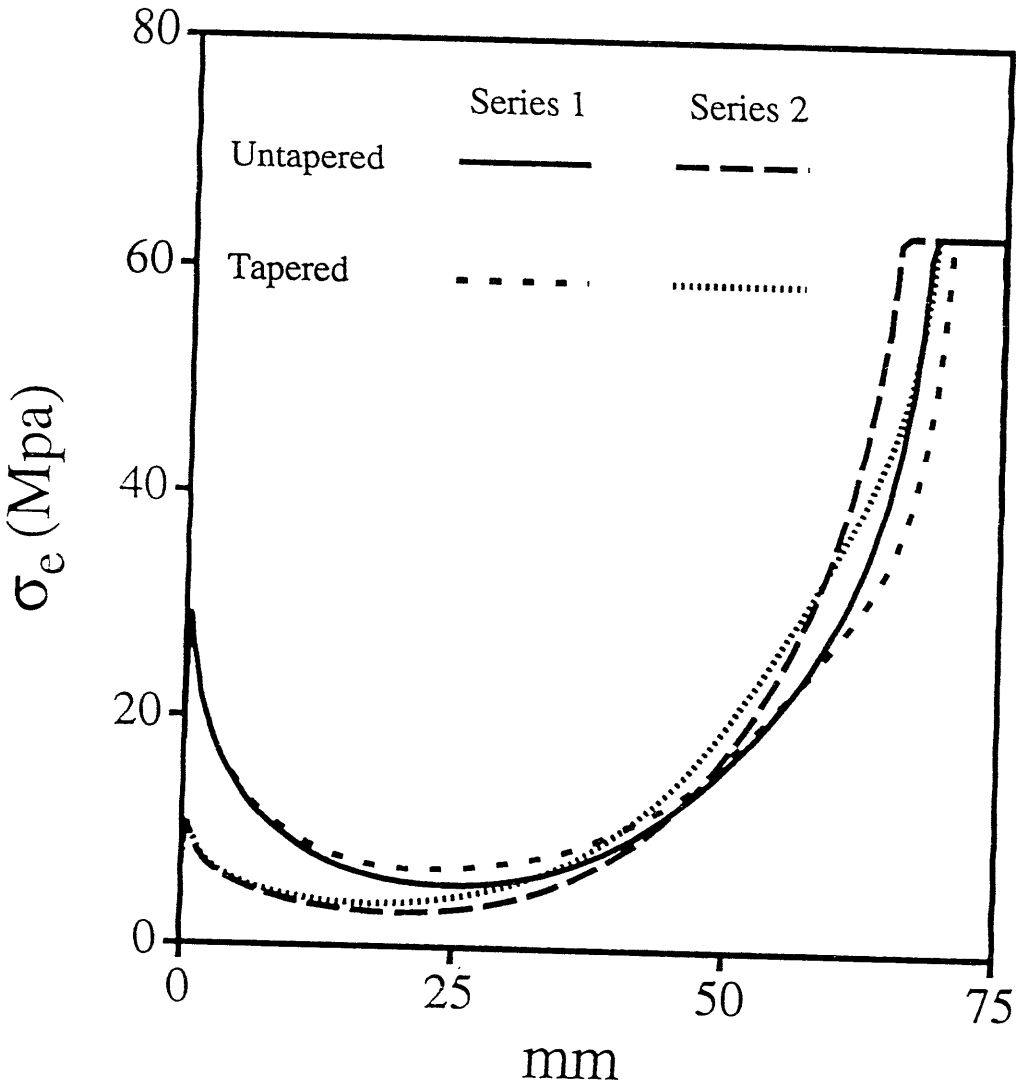

Fig. 7. Calculated effective (von Mises) stress distribution in adhesive as a function of metal adherend taper for Series 1 and 2 joints (τ = 10.6 MPa). Distance measured relative to outer bond end in elements adjacent to composite.

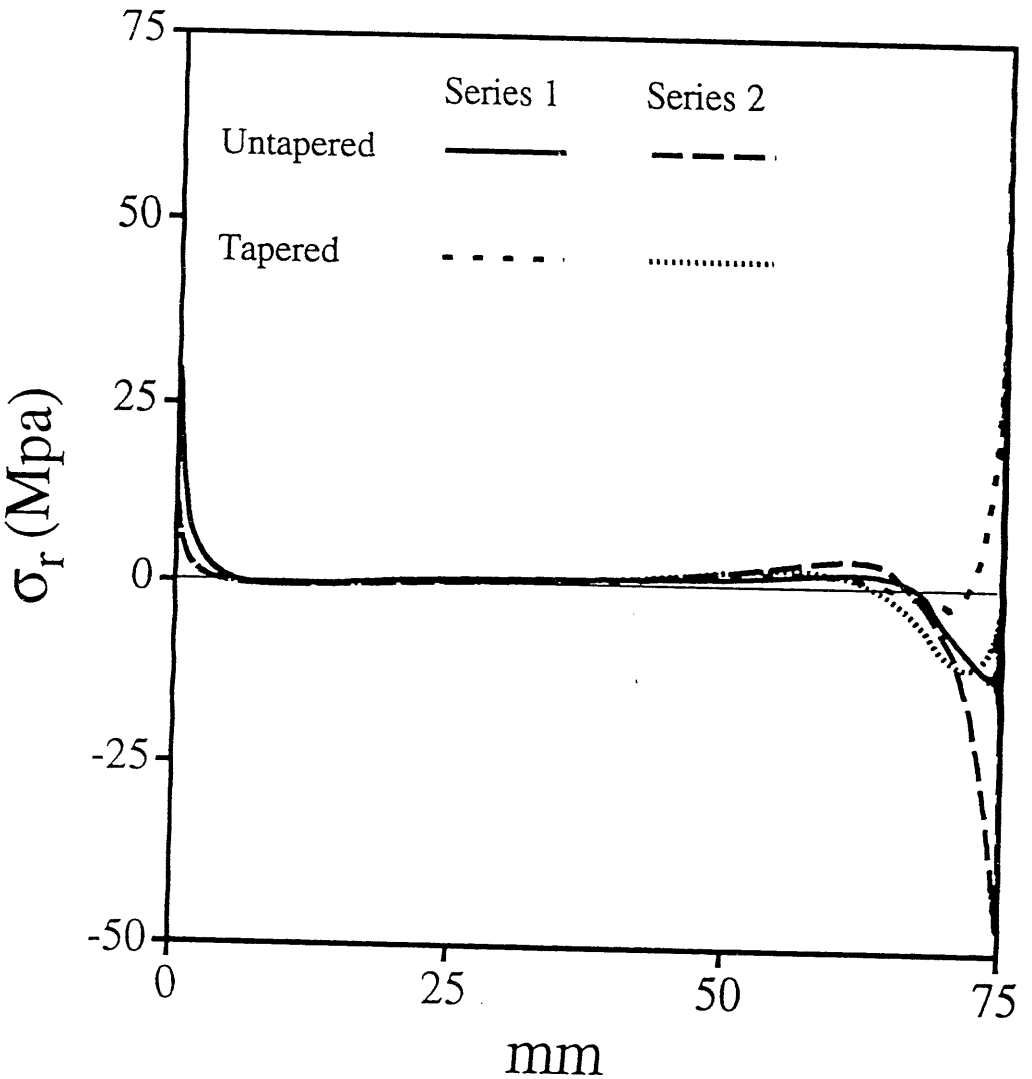

Fig. 8. Calculated radial stress distribution in adhesive as function metal adherend taper for Series 1 and 2 joints (joint loaded in tension and τ = 10.6 MPa).

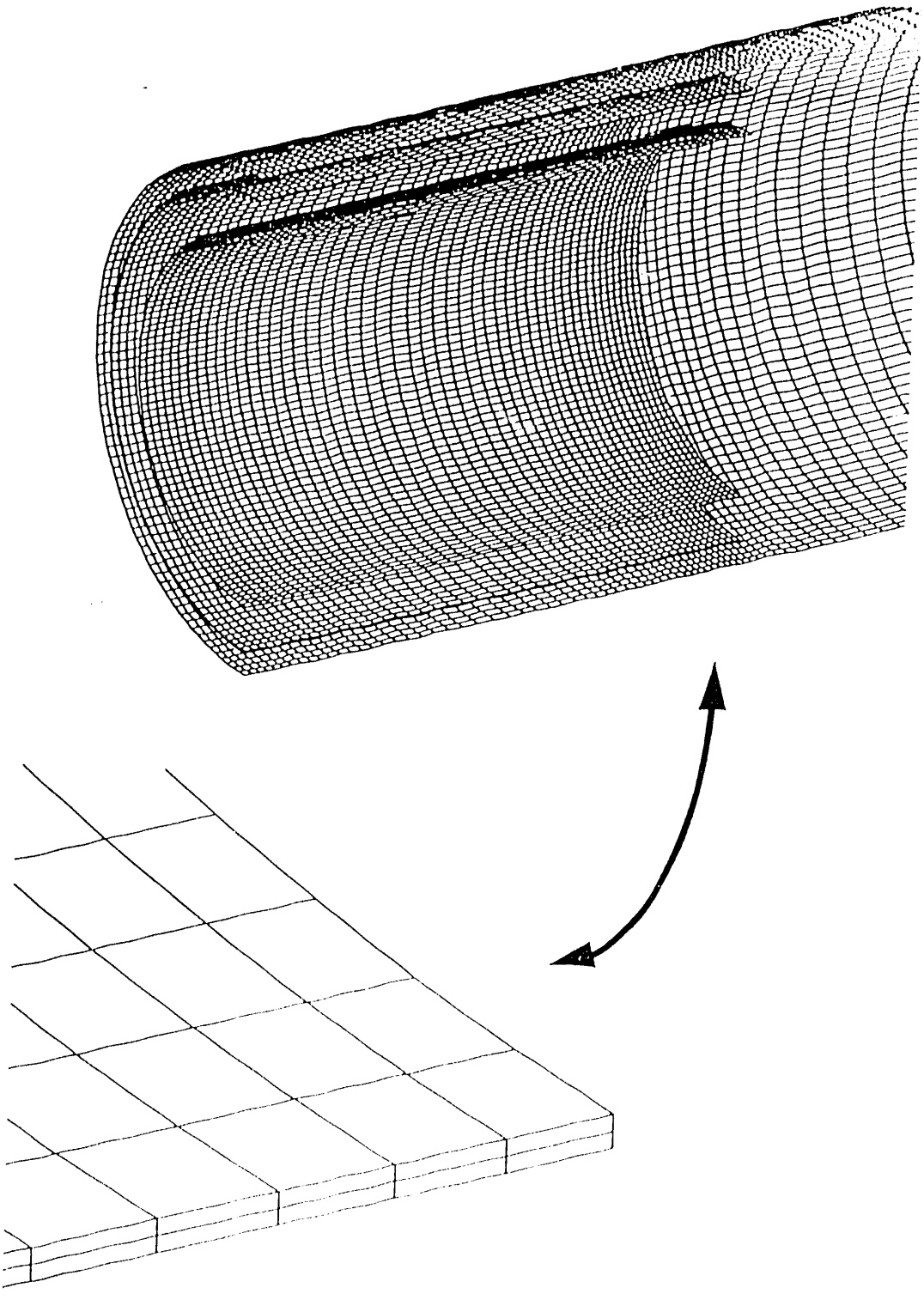

Fig. 9. Finite element model of the flexure joint specimen.

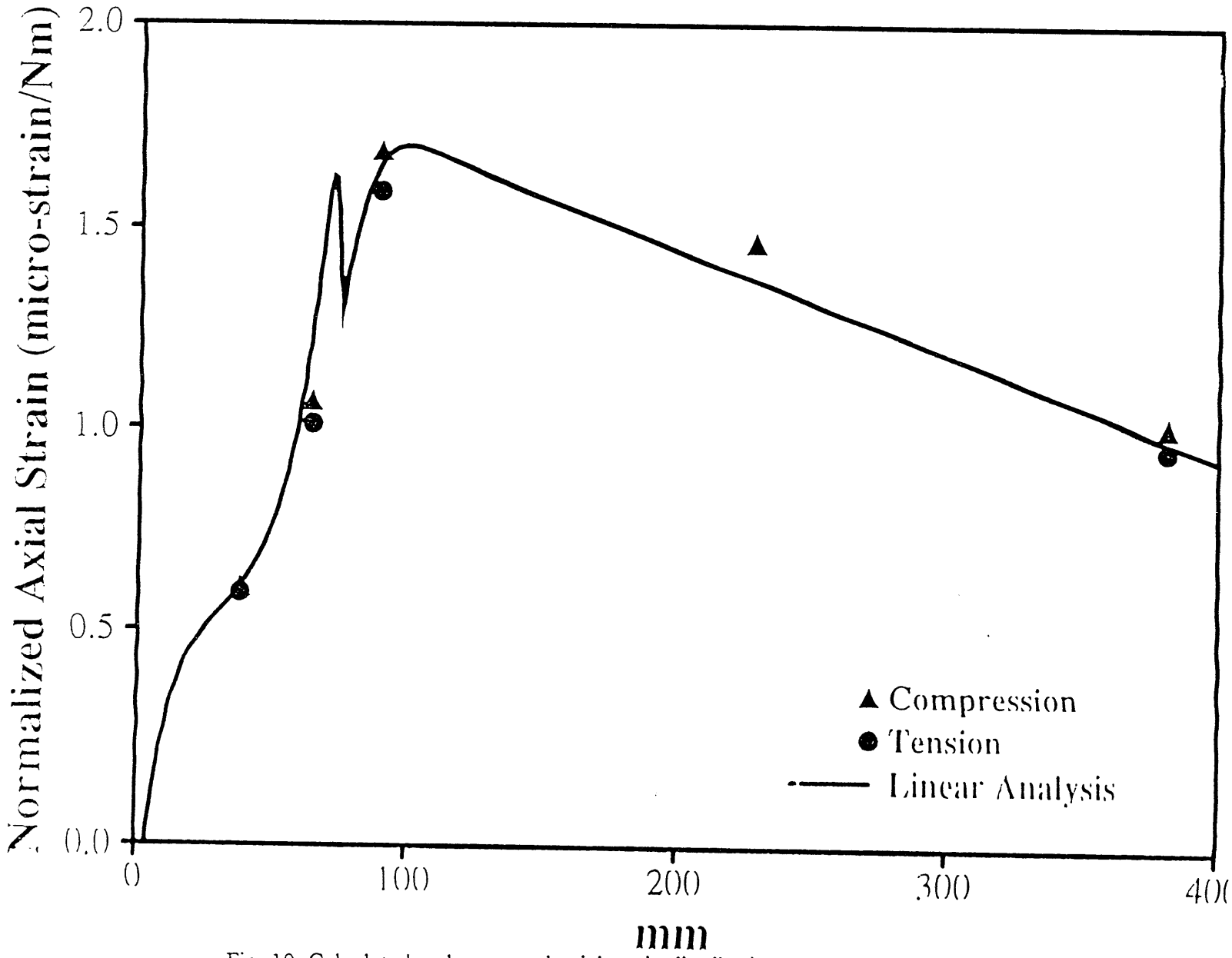

Fig. 10. Calculated and measured axial strain distribution along the outer E-glass adherend of the flexure joint specimen (moment = 328 Nm).

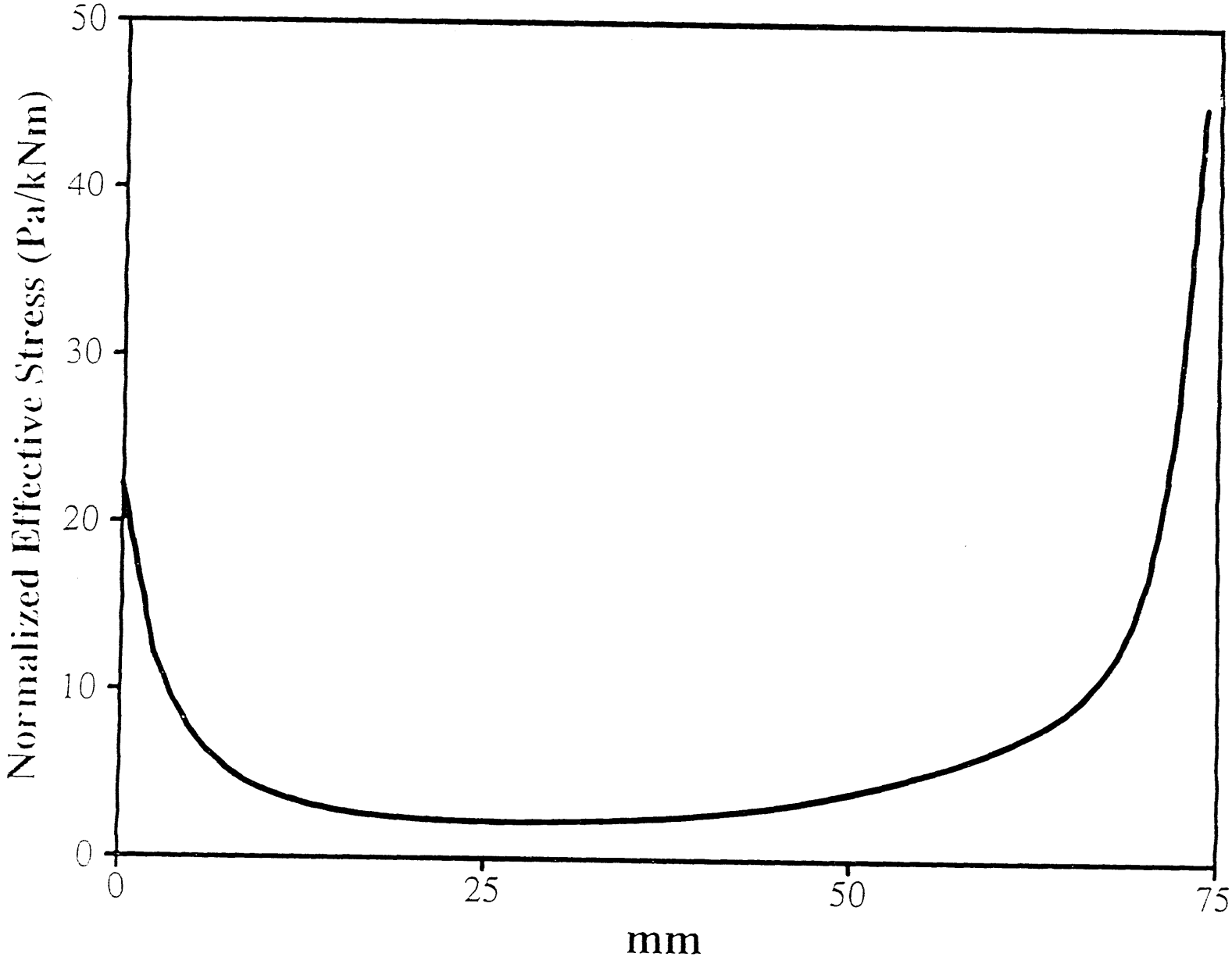

Fig. 11. Calculated effective (von Mises) stress distribution along the bond of the flexure joint specimen.

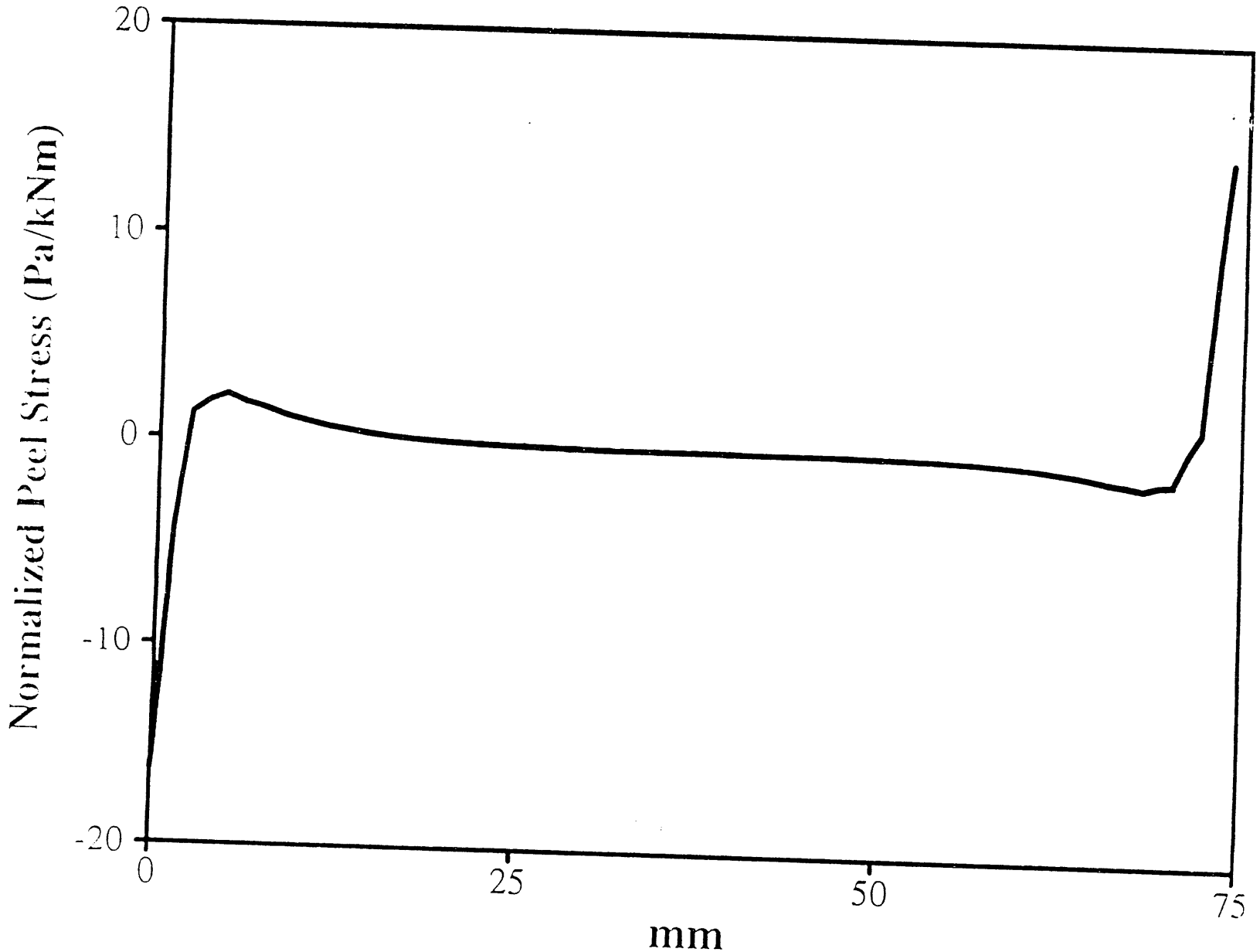

Fig. 12. Calculated peel (radial) stress distribution along the bond of the flexure joint specimen.

DATE
FILMED
1/11/94
END